Front. Optoelectron. China 2008, 1(1–2): 25–32
DOI 10.1007/s12200-008-0040-2

REVIEW ARTICLE

Guided properties and applications of photonic bandgap fibers

Zhi WANG (✉), Yange LIU, Guiyun KAI, Bo LIU, Chunshu ZHANG, Long JIN, Qiang FANG, Shuzhong YUAN, Xiaoyi DONG

Institute of Modern Optics, Nankai University, Tianjin 300071, China

Abstract The authors have reviewed some of their recent studies on photonic bandgap fibers (PBGFs). PBGFs that confine light in the core by the photonic bandgap effect of cladding have potential applications in various photonic devices. In this paper, the guided properties and tuned mechanics of anti-resonant PBGFs are theoretically illustrated. The special coupling properties in multi-core PBGFs, such as decoupling and resonant coupling effect, are then introduced. Finally, fiber Bragg grating inscribed in all-solid PBGFs is theoretically and experimentally studied, and special resonant characteristics are also observed.

Keywords photonic crystal fibers (PCFs), photonic bandgap, directional coupler, fiber Bragg grating

1 Introduction

In recent years, photonic crystal fibers (PCFs) have become more attractive due to unique properties such as endless single-mode guiding [1], high nonlinearity [2], and tailorable group velocity dispersion (GVD) [3]. PCFs can be commonly classified as index-guided PCFs, which guide light through total internal reflection (TIR), and photonic bandgap fibers (PBGFs), which guide light in a low-index core through the photonic bandgap (PBG) effect [4]. One of the most interesting PBGFs is the hollow-core PBGF, in which light can be confined in an air core by a periodic array of air holes in silica [5,6]. Hollow-core PBGFs have been widely studied in various applications such as gas nonlinearity [7], high power soliton delivery [8], and pulse compression [9]. Another kind of PBGF, the so called anti-resonant PBGF, is commonly composed of a solid core and a two-dimensional array of high-index rods in a silica background [10]. Anti-resonant PBGFs can be achieved by infiltrating the air-holes of TIR-PCFs with high-index liquid material. If the refractive index of the infiltrating material, such as liquid crystal, is sensitive to temperature or electric fields, the guided properties of the anti-resonant PBGFs will be tunable [11]. The all-solid PBGF, another kind of anti-resonant PBGF, is usually composed of a two-dimensional array of high-index germanium-doped silica rods in a pure silica background [12]. All-solid PBGFs are easier to fabricate and couple with conventional fibers than hollow-core PBGFs, and have potential applications in integrated fiber communication devices.

A study on PBGFs has been carried on by our research group in recent years [13–21]. This paper gives an overview of the progress of our work. In Sect. 2, the guided properties and design of anti-resonant PBGFs are demonstrated. Coupling properties of multi-core PBGFs are investigated in the next section. The fiber Bragg grating (FBG) inscribed in PBGFs is then shown in Sect. 4. Finally, conclusions are given in Sect. 5.

Received October 22, 2007; accepted November 17, 2007

E-mail: zhiwang@nankai.edu.cn

2 Guided properties of anti-resonant PBGFs

When high index materials such as liquid crystals are filled in the air holes of general TIR-PCFs, as shown in Fig. 1(a), the fiber cannot guide light by TIR since the fiber now has a low-index silica core surrounded by high-index rods. However, this infiltrated fiber can support a number of guided-wavelength bands due to the PBG effect formed by the anti-resonance in high index rods [13].

In Fig. 2, the bandgaps of the pattern are depicted by using the plane-wave method. In this case, the holes have diameter d and pitch length Λ of 1.8 and 3.38 μm, respectively. The refractive index of silica and infiltration material is assumed to be 1.444 and 1.653, respectively. The diagram reveals the existence of two PBGs and a silica line crossing the fundamental and secondary gap regions. For a specific propagation constant value, no fundamental modes are allowed to propagate in the anti-resonant PBGFs if their frequencies are not located in the PBGs and below the silica line.

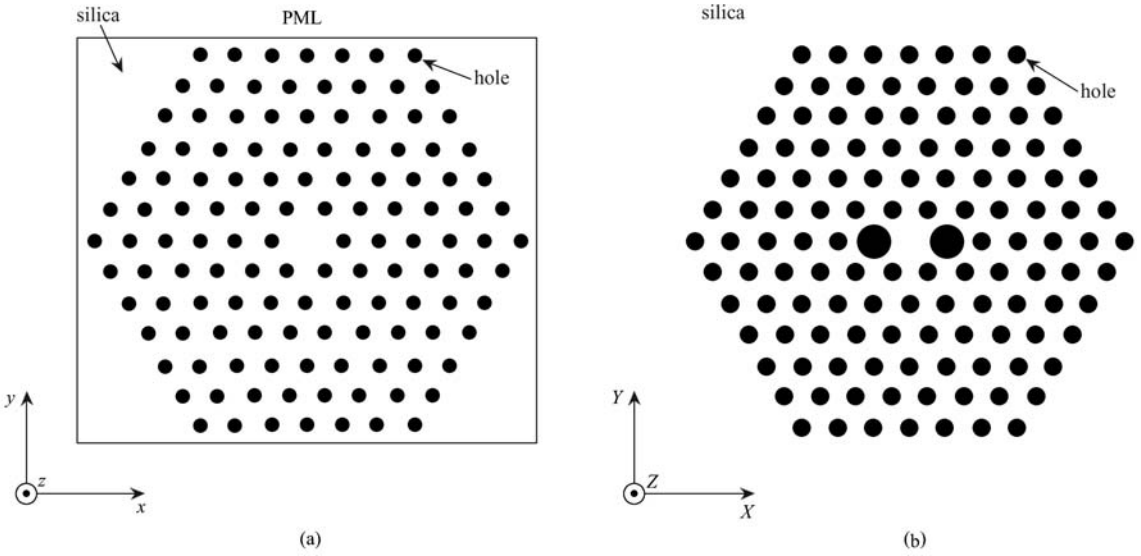

Fig. 1 Cross section of anti-resonant PBGFs. (a) Regular structure [13]; (b) high-birefringent structure [15]

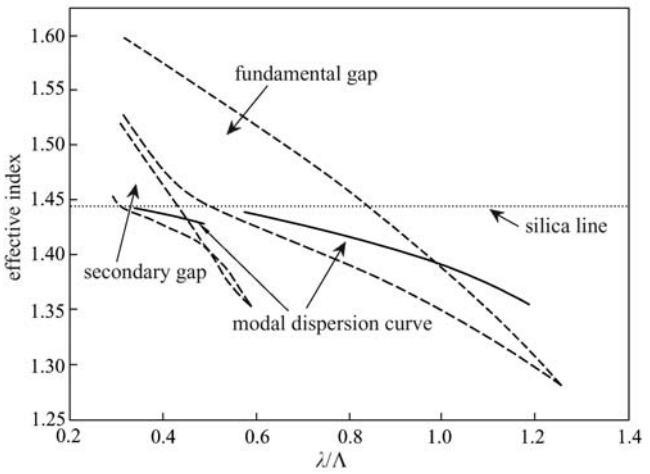

Fig. 2 Modal dispersion curve for the fundamental mode of anti-resonant PBGFs as a function of normalized wavelength [13]

Assuming that the anti-resonant PBGFs have an infinite number of air holes, light would be confined in the core region by a fully two-dimensional PBG and leakage losses would not occur. However, the number of air holes in the cladding is finite in practice, so the mode is leaky. Figure 3 shows the wavelength dependence of the normalized leakage loss of PCFs before and after they are filled with high-index material. As expected, the leakage loss becomes minimum around the center of the PBG and increases as it approaches the band edges after filling. This effect indicates that the mode fields are confined to the core of the fiber when the modes appear around the center of the PBG, but can enlarge the size of the cladding rapidly when the modes are close to the edges of the PBG.

Figure 4 shows the leakage loss and waveguide GVD (D_w) as a function of normalized wavelength for anti-resonant PBGFs with six periods of filled rods in fundamental PBG, where the refractive index of the

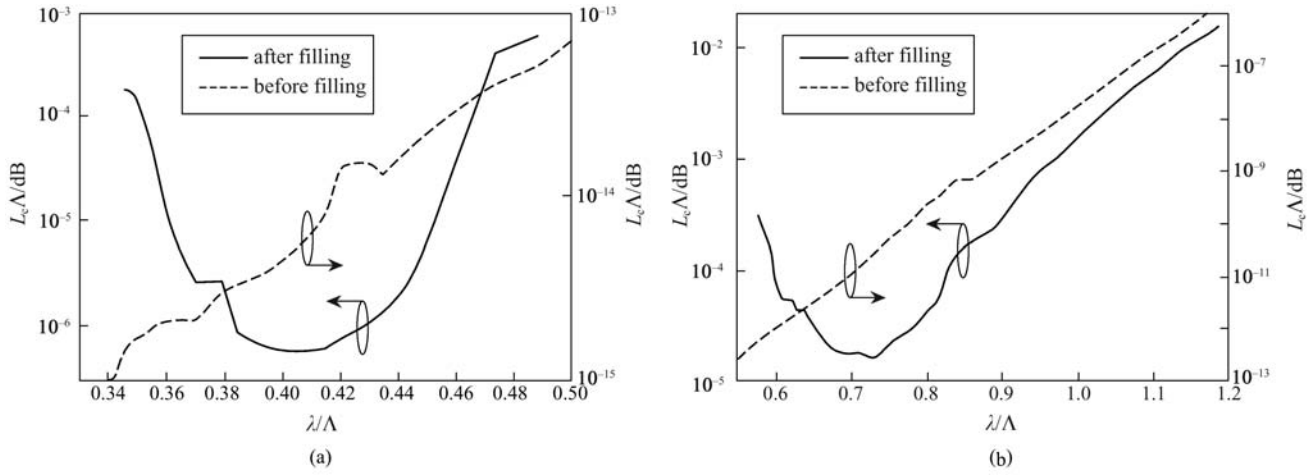

Fig. 3 Normalized leakage losses of the fundamental mode. (a) In the second bandgap; (b) in the fundamental bandgap [13]

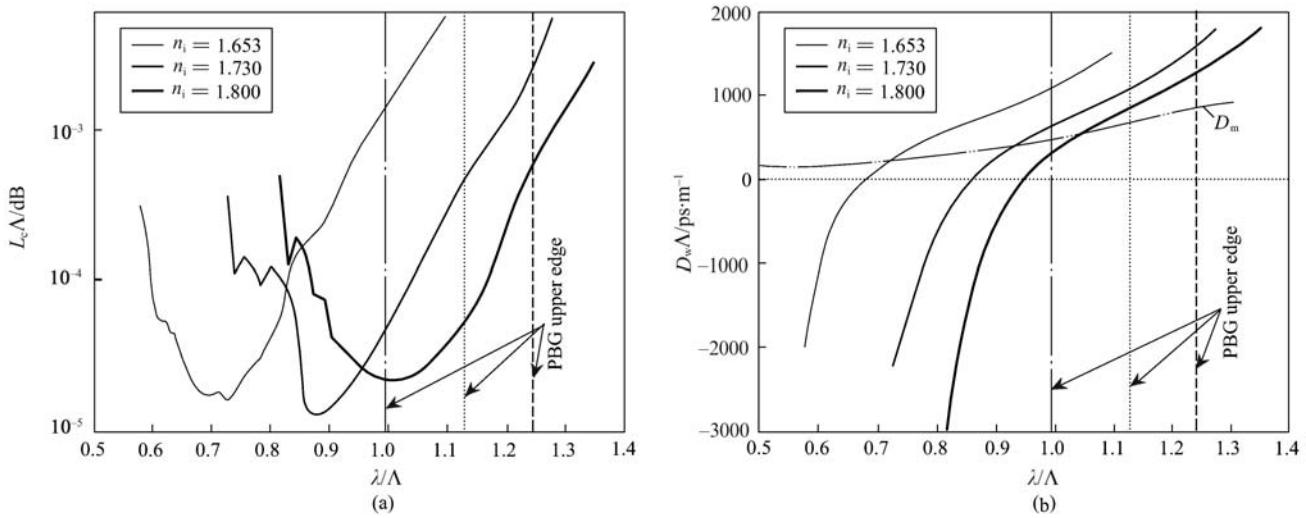

Fig. 4 Normalized leakage loss (a) and normalized waveguide GVD (D_w) (b) in the fundamental gap region when the refractive index of the filling material is 1.653, 1.73, and 1.80 (D_m denotes the material dispersion of silica) [17]

infiltration material n_i is taken as a parameter. According to Fig. 4(a), the leakage loss is slightly variable with the increasing n_i, although the variety brings a shifting of the PBG. According to Fig. 4(b), the waveguide GVD for various n_i exhibits the same qualitative behaviors as follows: a) the GVD is strongly wavelength-dependent; b) it changes from negative values at shorter wavelengths to positive values at longer wavelengths; c) it increases rapidly near the upper band edge and decreases rapidly near the lower band edge; d) it crosses the zero point within the low-loss window. However, there are still some differences when n_i is at different values. The dispersion slope around the center of PBG with a larger value of n_i is smaller than that of PBG with a smaller value of n_i. These results suggest the possibility of a tunable optical filter, switches and dispersion controller that can be designed with anti-resonant PBGFs by infiltrating tunable material.

Figure 1(b) shows the cross section of the typical high birefringent PCF, in which light is guided by TIR before high-index material fills the air holes [15]. The birefringence is caused by one pair of large air holes around the fiber core. When the air holes of the fiber are filled with a high-index material, the anti-resonant PBGF is formed. However, as shown in Fig. 5, not only the core guided modes, but also the guided modes located in the two large high-index rods near the core are found in PBG in this fiber. The avoided crossing between the core modes and rod modes will dominate the guided properties of the fiber, such as birefringence and dispersion. Figure 6 shows the polarization mode dispersion (PMD) of PBGFs with high birefringence, and the refractive index of infiltration material is taken as a parameter. Due to the avoided crossing effect, the PMD varies unconventionally around the wavelength region where the large rod modes strongly couple with the fundamental core modes.

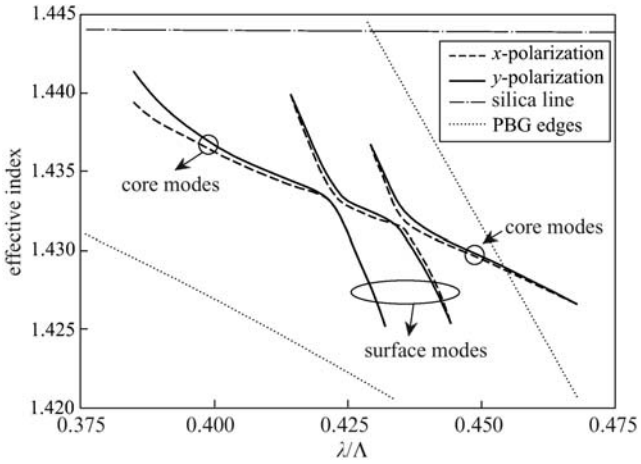

Fig. 5 Effective indices of two orthogonal polarization modes in birefringent PBGFs (refractive indices of high-index material is 1.653) [15]

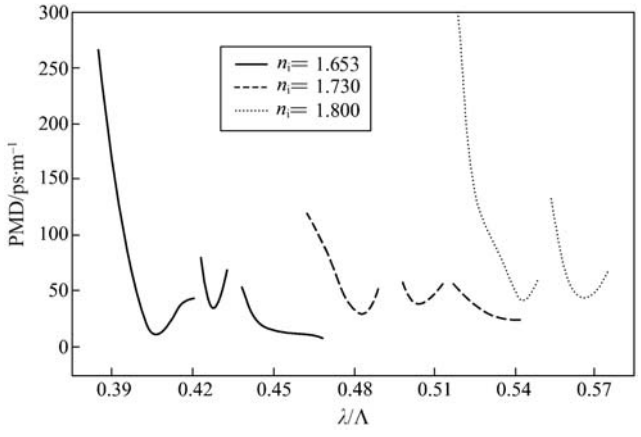

Fig. 6 Normalized wavelength dependence of PMD for PBGFs with high birefringence [15]

The avoided crossing effect in PBGFs can also be used to design the dispersion of the fiber. Since all-solid PBGFs have potential applications in photonic devices such as mode-lock fiber lasers, improve their dispersion characteristics has great significance in improving the performance of these photonic devices. Here, a novel design of all-solid PBGF is proposed, in which several bigger high-index rods are introduced, as shown in Fig. 7 [20]. In the fundamental PBG of the fiber, not only the core guided modes but also the high-order supermodes in the bigger rods are found. Since the dispersion curves of the core guided modes and the high-order supermodes have different slopes, the avoided crossing effect will occur when they have the same symmetry and polarization. As a result, large normal and anomalous dispersions are found near the avoided crossing wavelength in the center of the PBG. As Fig. 8 shows, due to the avoided crossing effect, these dispersions are also gained within the band-gap. Since the two dispersion slopes are different, the slope could be adjusted by introducing a different number of defect rods.

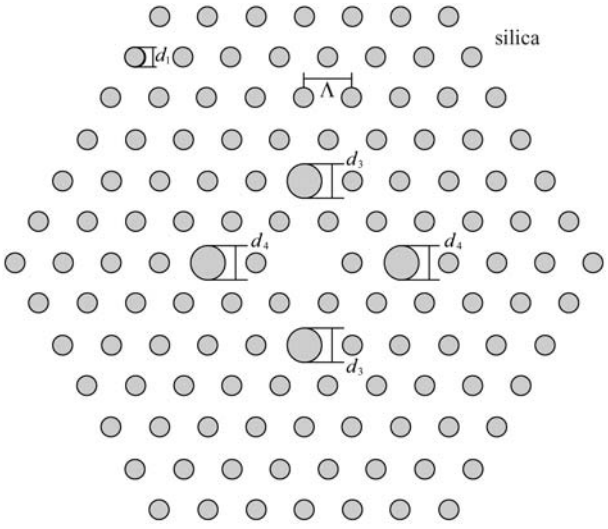

Fig. 7 Cross section of all-solid PBGF with several larger high-index rods [20]

3 Multi-core PBGFs

Multi-core PCFs are attractive due to their flexibility and easy design, with which they can be fabricated by using the stack and draw procedure. Due to special guided mechanisms, multi-core PBGFs can show some remarkable coupling properties such as decoupling, maxima and minima in coupling length, and resonant coupling. In dual-core fibers, the guided mode for each polarization in cores is split into two supermodes. Based on the parity of the mode field with respect to the geometric symmetry axis between two cores, these are referred to as the even and odd core-guided supermodes. The coupling length L_c

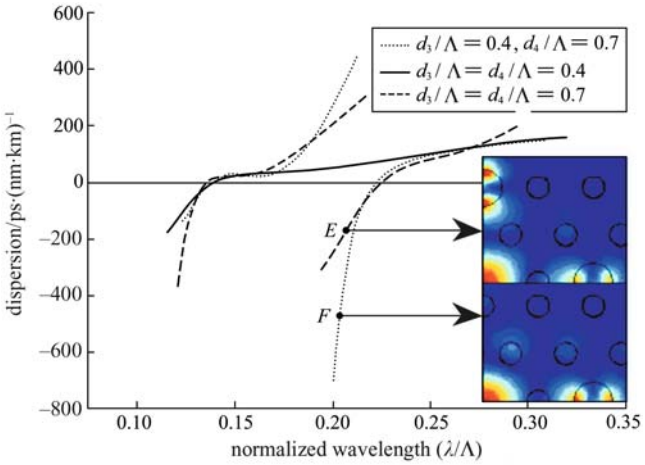

Fig. 8 Waveguide dispersion of core guided mode of all-solid PBGFs shown in Fig. 7 (the inset is the mode field of point *E*, *F*) [20]

is the distance along the fiber, in which there is a total transfer of power from one core to the other. L_c can be expressed as

$$L_c = \pi / \left(k \left| n^i_{\text{even}} - n^i_{\text{odd}} \right|\right), \quad i = x, y, \tag{1}$$

where n^i_{even} and n^i_{odd} are the effective index of *i*-polarized even and odd supermodes, respectively; $k = 2\pi/\lambda$ is the vacuum wave vector and λ is the wavelength in vacuum.

Decoupling means the coupling length is infinite and no power transfer occurs between the nearby waveguides. Decoupling can occur in dual-core PBGFs when the effective indexes of even and odd supermodes are equal. The cross section of the dual- and hollow-core PBGF structure considered here is shown in Fig. 9 [14]. In the cross section of the PBGFs, two larger air holes are introduced into the

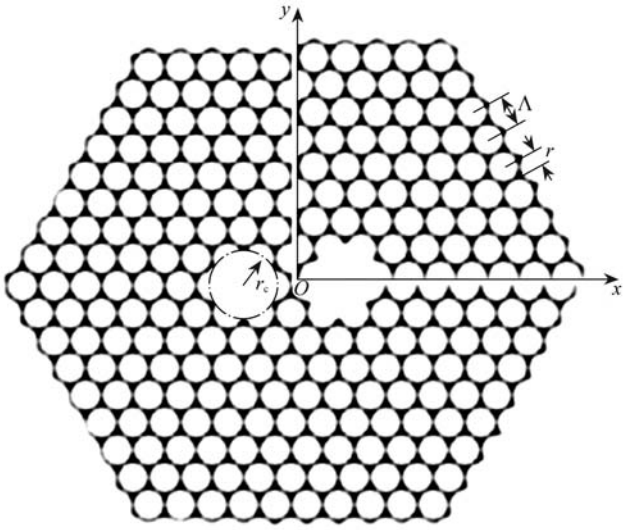

Fig. 9 Cross section of dual- and hollow-core PBGF (Λ and *r* are the pitch and radius of the air holes in cladding, respectively, r_c is the radius of the two defect cores) [14]

photonic crystal cladding with a triangular lattice pattern of air holes as the defect cores. The air hole radius $r = 0.47\Lambda$, where Λ is the pitch of the air holes, and the radius for the two defect cores is r_c.

Figure 10 shows the effective indices n_{eff} of guided modes and PBG edges as a function of normalized wavelength λ/Λ with $r_c = 1.05\Lambda$. Two eigenmodes, even and odd supermodes, appear inside the PBG for each polarization direction. As show in Fig. 10, for y-polarization, the effective index of the even supermode is higher than that of the odd supermode for every wavelength. For x-polarization, the dispersion curves of even and odd supermodes intersect at $\lambda = 0.632\Lambda$ and the odd supermode has a higher effective index than the even supermode in the wavelength range over the crossing point. At the crossing point, the propagation constant of the even supermode is the same as that of the odd supermode and the dual-core PBGF is decoupled. Figure 11 shows the wavelength dependence of normalized coupling length L_c/Λ for both polarizations. The value of coupling length for x-polarization decreases slightly from $\lambda = 0.563\Lambda$ to $\lambda = 0.569\Lambda$, then increases dramatically from 869Λ at $\lambda = 0.569\Lambda$ to infinity at $\lambda = 0.632\Lambda$. The value of L_c decreases rapidly as the wavelength increases in the wavelength range over the crossing point.

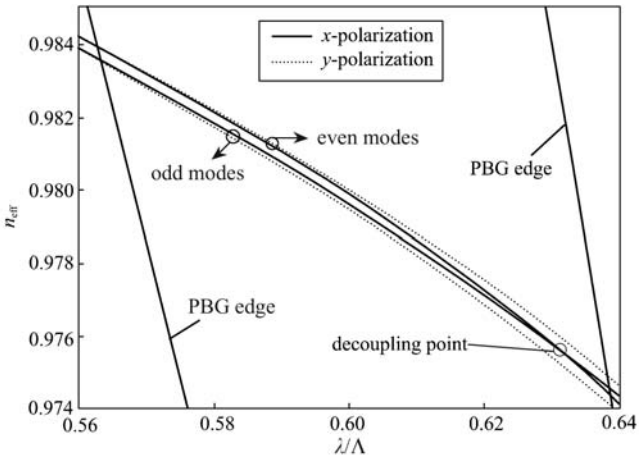

Fig. 10 Effective index of PBG edges and defect mode in dual-core PBGF [14]

Decoupling means the dispersion curves of odd and even supermodes can intersect with each other. The even supermode is a fundamental mode and always has a higher effective index than its odd counterpart in dual-core index-guided fibers. Since the fundamental modes of the individual cores have a positive phase everywhere, their overlaps are always positive [18]. As a result, the decoupling never occurs in these fibers. Whereas PBG guided core modes are not fundamental mode in PBGFs, and the parity of the high index supermode depends on the symmetry of the cladding modes in the photonic band at the PBG edges and the arrangement of

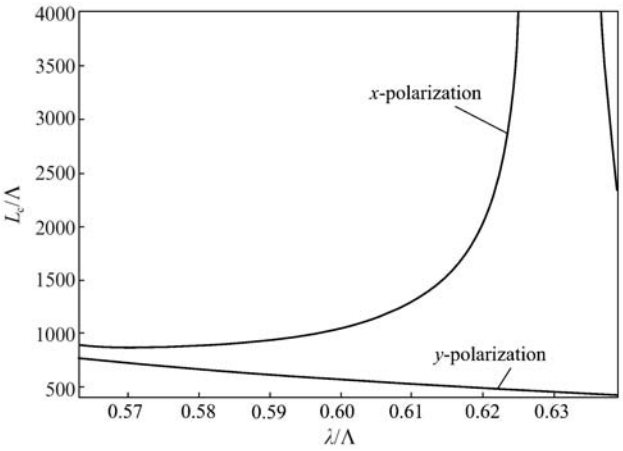

Fig. 11 Normalized coupling length of dual-core PBGF [14]

two cores [18]. If the parity of the high index supermode at two edges of the PBG is different, the dispersion curves of odd and even supermodes will intersect each other in the PBG, and decoupling occurs. Decoupling can not only be found in hollow-core PBGFs, but also in all-solid PBGFs. Dual-core all-solid PBGFs have been fabricated by Wang Z, et al. in the University of Bath and decoupling has also been experimentally observed in these fibers [18].

Directional couplers operated by resonance can be realized by introducing some defects between the two cores in PBGF. When the avoided-crossing effect between defect-guided modes and core-guided supermodes occurs, energy transfer enabled by these defects function as a transverse resonator [22]. Here the design of the directional coupler operated by resonant coupling is numerically presented based on all-solid PBGFs [19]. The directional couplers consist of a cladding with an array of high-index rods in silica background, two cores formed by omitting two rods, and some defect rods introduced by reducing the diameters of the high-index rods between two cores, as shown in Fig. 12 [19]. The background material is silica with an index of 1.457, and the circles denote the raised-index rods formed

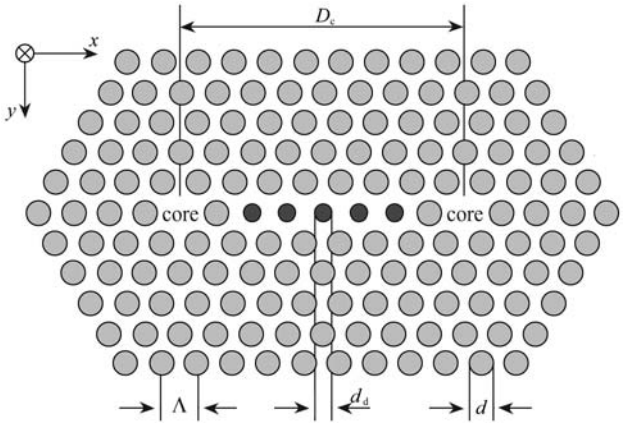

Fig. 12 Schematic diagram of directional coupler based on all-solid PBGFs [19]

by germanium-doped rods with an index of 1.47288. The rod diameter d is 0.7Λ, where Λ is the rod pitch. The diameter of the defect rods $d_d = 0.75d$. The resonant effect between the LP_{01}-like core supermodes and higher order defect guided modes are found in this fiber.

The normalized coupling length of dual-core all-solid PBGFs with and without the resonant defect is shown in Fig. 13. From Fig. 13, it can be seen that the curves of normalized coupling length are significantly different for the fiber with and without the defect rod, although the difference between the two structures is slight. When the defect rod is introduced, power can transfer between the cores through the rod and the normalized coupling length would obtain its minimum at the resonant point. As a result, the normalized coupling length becomes observably shorter than that in the fiber without resonant defect. Note that due to low index contrast, the difference of the coupling length between x and y polarization is very small. The resonant effect makes the coupling length significantly decrease, which makes it possible to realize applications for more complex communication devices. Some important fiber components in communication systems such as the FBG and fiber amplifier could be introduced in the structures for integrated all-fiber devices.

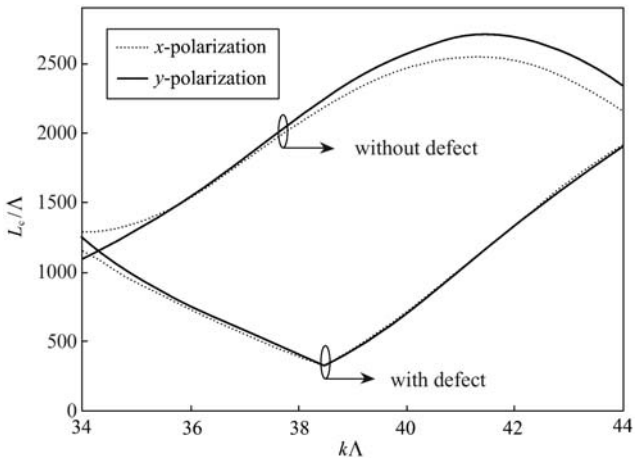

Fig. 13 Normalized coupling length L_c/Λ as a function of normalized frequency $k\Lambda$ in the PBGFs with and without resonant rod in the case of $D_c = 4\Lambda$ [19]

4 FBG inscribed in PBGFs

FBG is formed by periodic index modulation in the core of a step-index fiber along the fiber length, which can couple light to the discrete core, cladding modes and continuous radiation modes. Due to the incorporation of Ge-doped rods, it is feasible to photo-inscribe the fiber gratings into all-solid bandgap fibers effectively. The Bragg grating inscribed in the all-solid bandgap fiber not only has potential applications in communication and sensor devices, but can also be used to study the properties of modes in bandgap fibers [21].

Figure 14 shows the microscope photograph of the cross section for the all-solid bandgap fiber. The fiber was fabricated by Bath University using a modified stack-and-draw process. The guided modes and bandgaps of the fiber are plotted in Fig. 15. It is shown that C-band of around 1550 nm is included in the fundamental bandgap located between the LP_{01} and LP_{11} supermode band cut-offs. The spatial field distribution of the core mode in the inset of Fig. 15 shows a small fraction of energy distributed in the inner ring of high-index rods. Therefore, grating resonances between guided mode and supermodes at certain wavelengths are possibly produced by index modulation over the high-index rods.

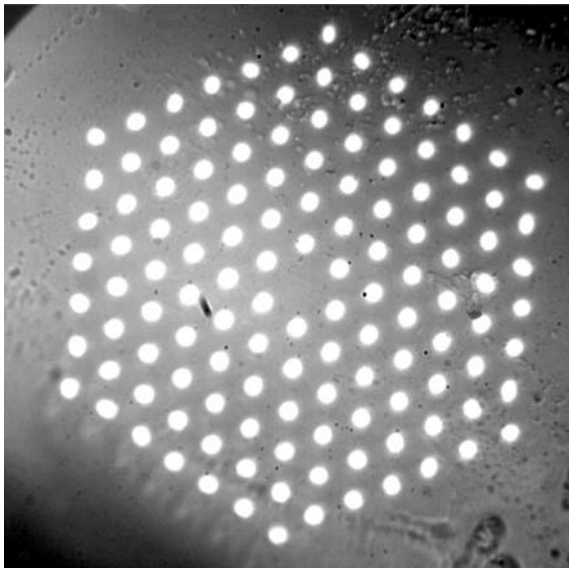

Fig. 14 Microscope photograph of the facet for all-solid bandgap fiber (the bright spots are embedded Ge-doped rods)

The all-solid PBGF spliced with single mode fibers is loaded in hydrogen atmosphere at 100°C for 48 h to enhance its photosensitivity. The bandgap fiber is then exposed by focused pulses from a 248 nm KrF excimer laser. The grating period is 1065 nm and the grating length is 1.3 cm. Figure 16 shows the transmission and reflection spectra of the FBG, from which peaks A (1540.58 nm, 4.4 dB) and B (1537.8 nm, 1.1 dB) are observed. However, only dip B finds its corresponding reflective peak in the reflection spectrum. Since the guided mode has the largest overlap with single mode fibers among all the modes, it can be shown that peak B arises from the coupling between forward and backward core guided modes. The resonant wavelength of peak A is longer than peak B, indicating that peak A arises from coupling to supermodes which have higher effective indices than that of the core mode. As shown in Fig. 15, only LP_{01} supermodes can satisfy this condition. Therefore,

peak A corresponds to coupling to LP_{01} supermodes. Grating resonance to the mode with a higher effective index than fundamental core mode was only observed in our experiment due to the specific modal distribution in the all-solid PBGFs. The resonant wavelengths for peaks A and B are calculated and shown in Fig. 16. Simulated resonant wavelengths for forward and backward core modes (blue line) and for core modes and LP_{01} supermodes band (region between red lines) are also shown in the figure. The calculated wavelengths of peaks A and B are in good agreement with the experimental results. The small deviations between the calculated and measured values come from the uncertainty of the transverse structure parameter of the fiber.

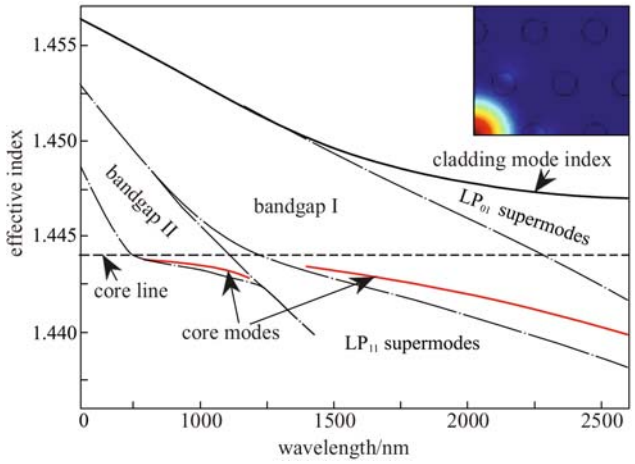

Fig. 15 Core modes and bandgaps of all-solid bandgap fiber (inset: the spatial filed distribution of the core mode at 1540 nm) [21]

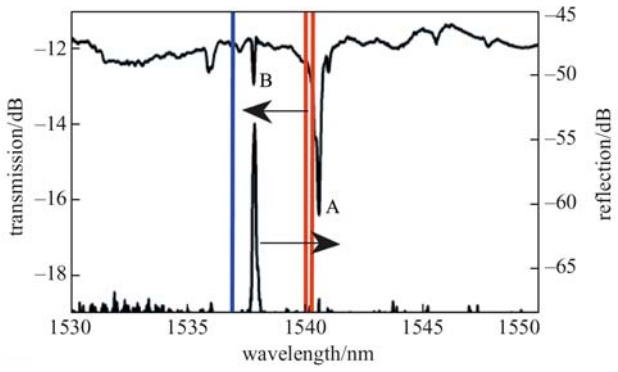

Fig. 16 Transmission and reflection spectrum of FBG in all-solid bandgap fiber [21]

5 Conclusions

PBGFs have exhibited their potential applications in various photonic devices. The anti-resonant PBGFs, obtained by filling the holes of the TIR-PCFs with high-index materials, can be used as tunable devices. Their guided properties, such as loss, GVD and birefringence, can be tuned by varying the refractive index of the filled materials. The GVD of the all-solid PBGFs can be designed by introducing an additional effect. The multi-core PBGFs can present some special coupling properties, such as decoupling and the resonant coupling effect. These fibers can be used as basic components of the complex integrating all-fiber communication devices. The FBGs inscribed in all-solid PBGFs exhibit special spectral characteristics. Therefore they can not only have potential applications in fiber communication and sensing, but can also be used to study the modal properties of PBGFs.

Acknowledgements This work was supported by the National Basic Research Program of China (973 project, Grant No. 2003CB314906), the National Nature Science Foundation of China (Grant No. 10674074), the Tianjin Natural Science Foundation Project of China (Grant No. 06YFJZJC00300), the 863 National High Technology Programme of China (Grant No. 2006AA01Z217) and the Open Project Foundation of Key Laboratory of Opto-electronic Information Science and Technology, Ministry of Education, Nankai University (Grant No. 206006).

References

1. Birks T A, Knight J C, Russell P S J. Endlessly single-mode photonic crystal fiber. Optics Letters, 1997, 22(13): 961–963
2. Knight J C, Arriaga J, Birks T A, et al. Anomalous dispersion in photonic crystal fiber. IEEE Photonics Technology Letters, 2000, 12(7): 807–809
3. Broderick N G R, Monro T M, Bennett P J, et al. Nonlinearity in holey optical fibers: measurement and future opportunities. Optics Letters, 1999, 24(20): 1395–1397
4. Knight J C. Photonic crystal fibres. Nature, 2003, 424(6950): 847–851
5. Cregan R F, Mangan B J, Knight J C, et al. Single-mode photonic band gap guidance of light in air. Science, 1999, 285(5433): 1537–1539
6. Couny F, Benabid F, Light P S. Large-pitch kagome-structured hollow-core photonic crystal fiber. Optics Letters, 2006, 31(24): 3574–3576
7. Benabid F, Knight J C, Antonopoulos G, et al. Stimulated Raman scattering in hydrogen-filled hollow-core photonic crystal fiber. Science, 2002, 298(5592): 399–402
8. Ouzounov D G, Ahmad F R, Müller D, et al. Generation of megawatt optical solitons in hollow-core photonic band-gap fibers. Science, 2003, 301(5640): 1702–1704
9. Limpert J, Schreiber T, Nolte S, et al. All fiber chirped-pulse amplification system based on compression in air-guiding photonic bandgap fiber. Optics Express, 2003, 11(24): 3332–3337
10. Litchinitser N M, Abeeluck A K, Headley C, et al. Antiresonant reflecting photonic crystal optical waveguides. Optics Letters, 2002, 27(18): 1592–1594
11. Litchinitser N M, Dunn S C, Steinvurzel P E, et al. Application of an ARROW model for designing tunable photonic devices. Optics Express, 2004, 12(8): 1540–1550
12. Argyros A, Birks T A, Leon-Saval S G, et al. Guidance properties of low-contrast photonic bandgap fibres. Optics Express, 2005, 13(7): 2503–2511
13. Zhang C S, Kai G Y, Wang Z, et al. Transformation of a transmission mechanism by filling the holes of normal silica-guiding

microstructure fibers with nematic liquid crystal. Optics Letters, 2005, 30(18): 2372–2374
14. Wang Z, Kai G Y, Liu Y G, et al. Coupling and decoupling of dual-core photonic bandgap fibers. Optics Letters, 2005, 30(19): 2542–2544
15. Zhang C S, Kai G Y, Wang Z, et al. Tunable highly birefringent photonic bandgap fibers. Optics Letters, 2005, 30(20): 2703–2705
16. Zhang C S, Kai G Y, Wang Z, et al. Simulations of effect of high-index materials on highly birefringent photonic crystal fibres. Chinese Physics Letters, 2005, 22(11): 2858–2861
17. Zhang C S, Kai G Y, Wang Z, et al. Design of tunable bandgap guidance in high-index filled microstructure fibers. Journal of the Optical Society of America B–Optical Physics, 2006, 23(4): 782–786
18. Wang Z, Taru T, Birks T A, et al. Coupling in dual-core photonic bandgap fibers: theory and experiment. Optics Express, 2007, 15(8): 4795–4803
19. Wang Z, Liu Y G, Kai G Y, et al. Directional couplers operated by resonant coupling in all-solid photonic bandgap fibers. Optics Express, 2007, 15(14): 8925–8930
20. Fang Q, Wang Z, Kai G Y, et al. Proposal for all-solid photonic bandgap fiber with improved dispersion characteristics. IEEE Photonics Technology Letters, 2007, 19(16): 1239–1241
21. Jin L, Wang Z, Fang Q, et al. Bragg grating resonances in all-solid bandgap fibers. Optics Letters, 2007, 32(18): 2717–2719
22. Skorobogatiy M, Saitoh K, Koshiba M. Transverse lightwave circuits in microstructured optical fibers: resonator arrays. Optics Express, 2006, 14(4): 1439–1450